PAPER M

2.9-D CROSSWELL TRAVELTIME TOMOGRAPHY

Jessé Costa, Jerry Harris & Mark Van Schaack

ABSTRACT

The acquisition geometry of the multiple crosswell surveys used in the second phase of the McElroy Reservoir Geosciences Project provides the opportunity of reconstructing a 3-D slowness model from crosswell traveltime data. This led us to implement a 3-D traveltime inversion algorithm slowness reconstruction. The model is parameterized by the slowness values at nodes on a prismatic mesh. The slowness field is estimated from the joint inversion of the arrival times from the multiple crosswell surveys.

INTRODUCTION

The fundamental goal of reservoir characterization is to obtain 3-D information of the reservoir poro-permeability. Potentially these properties can be estimated from the acoustic properties of the rock providing hope that seismic imaging methods may help in reservoir characterization problems. Traditional crosswell traveltime tomography produces only a slice of the slowness field between two wells. Tomograms are typically computed independently for each survey even when multiple surveys are available (Mathisen et al., 1995). Unfortunately the 2-D assumption and inversion non-uniqueness often lead to tomograms that do not correlate satisfactorily in common wells. Crosswell data, however, is the highest frequency seismic data available at the interwell scale. Any attempt at high resolution seismic reservoir characterization, at this scale, should provide a consistent way to process multiple crosswell data sets to obtain 3-D information.

Joint inversion of multiple crosswell surveys for a 3-D slowness model requires prior information in order to ensure a well posed problem. The finest scale of inhomogeneity allowed in the solution must be limited in order to compensate for the lack of uniform volumetric ray coverage. The model parameterization using nodes (Harris, 1993) is a natural way to impose this constraint. This parameterization allows variations in model slowness that are very nearly 3-D in character. For this reason we have named the approach "2.9-D" tomography.

The construction of our 2.9-D inversion algorithm is based on a nodes parameterization of the slowness field and full 3-D ray tracing. The 3-D raytracing is an extension of the bending method using β-splines (Moser at al, 1992). The non-linear inversion is solved through successive linearizations. Additional regularization constraints reinforce the solution's lateral smoothness. The regularization weight is relaxed during the iterations following the continuation method (Bube and Langan, 1994).

3-D modeling allows us to overcome some of the difficulties found in traditional crosswell tomography. One advantage provided in a 3-D inversion is the ability to use the exact well geometries. Traditional 2-D crosswell tomography requires a projection to reduce the 3-D geometry of the experiment, which comes as a result of deviated wells, to a 2-D geometry. This procedure typically results in some inaccuracies. An exact representation of the source and receiver acquisition geometry can help reduce the types of artifacts that will result from these inaccuracies.

While the nodes parameterization can be an effective way to parameterize a model it is not completely general. A nodes parameterization assumes that a model with smooth lateral variations is sufficient to describe the data. Whenever the smooth lateral variations assumption is justified, this approach estimates a 3-D slowness model consistent with the true acquisition geometry and the entire data set.

FORWARD MODELING

Model parameterization

Our 3-D slowness model is defined at the nodes of a prismatic mesh as indicated in Figure 1. The slowness value at any point inside a triangular prismatic cell, $s(x,y,z)$, is interpolated using the six corner slowness values of that cell. Barycentric interpolation at the top and bottom of the cell is followed by linear interpolation in the vertical direction. This process is defined mathematically in Equation 1.

$$s(x,y,z) = \sum_{i=1}^{3} w_i(\mathbf{x}) \left[\frac{(z - z_t)}{(z_b - z_t)} s(x_i, y_i, z_t) + \frac{(z_b - z)}{(z_b - z_t)} s(x_i, y_i, z_b) \right]$$

$$w_i(\mathbf{x}) = \frac{(\mathbf{x} - \mathbf{x}_j) \times (\mathbf{x} - \mathbf{x}_k)}{(\mathbf{x}_i - \mathbf{x}_j) \times (\mathbf{x}_i - \mathbf{x}_k)} \quad \text{with } i \neq j \neq k;\ i,j,k = 1,2,3 \text{ and } \mathbf{x} = (x,y) \tag{1}$$

In Eqn. 1 x, y and z are defined using Cartesian coordinates, $\mathbf{x}_i$ indicates the (x,y) coordinates of the prism corners, and the subscripts t and b denote the cell's top and bottom.

The nodes parameterization offers two important advantages. First, it is possible to control the scale of inhomogeneity allowed by adjusting the distance between adjacent nodes. Second, the number of parameters defining the model is considerably less than normally required using rectangular pixels.

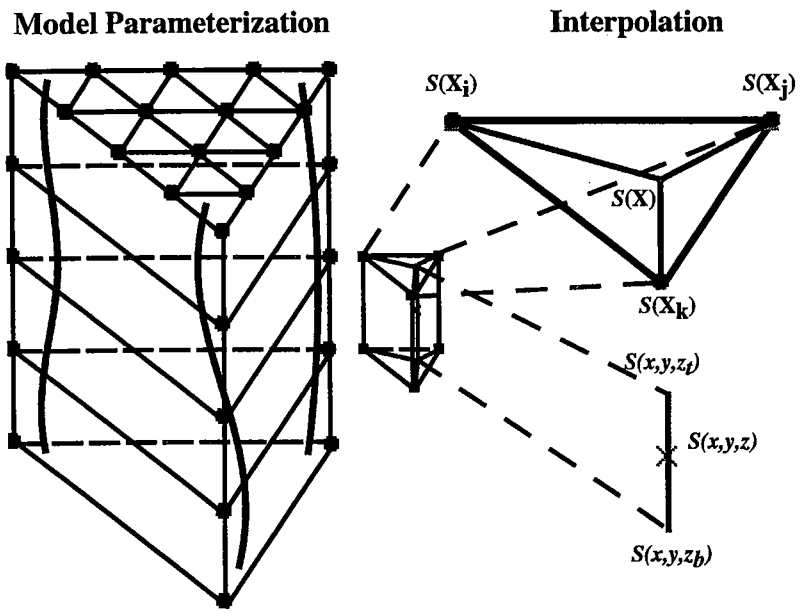

Figure 1. Model parameterization for 2.9-D tomography. The detail shows a cell and the interpolation scheme. Barycentric interpolation, defined in Eqn. 1, is performed at the top and bottom of the cell, followed by linear interpolation in the vertical direction.

Raytracing

Two point raytracing between source and receiver is solved by parameterizing the ray with cubic β-splines and using Fermat's principle to obtain the spline coefficients in a straightforward extension of Moser et al. (1992) to 3-D. The raypath is represented in the form,

$$\mathbf{X} = \sum_{v=1}^{N_v+1} \sum_{i=1}^{4} \mathbf{X}_{v-i} b_i(u) \qquad \text{with } u \in [0,1], \tag{2}$$

where $\mathbf{X}_v = (x_v, y_v, z_v)$ is the vector of β-spline polygon vertices and $b_i(u)$ is the vector of β-spline basis functions. The computation of the raypath between two points,

$\mathbf{X}_s$ and $\mathbf{X}_r$, is reduced to determining the vertices coordinates, $\mathbf{X}_v$, using Fermat's principle,

$$\underset{\mathbf{X}_v}{Min} \quad \tau(\mathbf{X}_v) = \int_{\mathbf{X}_s}^{\mathbf{X}_r} s(\mathbf{X}) d\mathbf{X}. \tag{3}$$

This problem is solved using conjugate gradients (Press et al., 1992). Our method provides a robust approach for obtaining 3-D raypaths with the typical trade-off between speed and accuracy. This trade-off is controlled through the choice of the number of vertices in the β-spline polygon. More vertices results in a higher degree of accuracy but also more computational time. In the work presented in this paper we use 21 vertices. The manner in which this value was chosen was to compare the percent traveltime difference for rays calculated in a test model using different numbers of vertices and then to chose the optimal value.

INVERSE PROBLEM

Regularization

Our 2.9-D tomographic inversion is solved iteratively through linearization. To stabilize the inversion, regularization constraints are imposed on the solution. The regularization is introduced through two regularizing functionals. These functionals are defined using the first derivative of the slowness field (1) in the horizontal plane and (2) in the vertical direction. Equation 4 defines the regularized objective function used in our 2.9-D tomographic inversion. Within this objective function the regularizing functionals act to minimize the inhomogeneities in the solution.

$$\underset{\mathbf{s}}{Minimize} \quad \left\| \tau_{obs} - \tau_{calc}(\mathbf{s}) \right\|_2^2 + \lambda_1^2 \left\| \mathbf{D}_x \mathbf{s} \right\|_2^2 + \lambda_2^2 \left\| \mathbf{D}_z \mathbf{s} \right\| \tag{4}$$

In Eqn. 4 τ_{obs} is a vector with the measured traveltimes, τ_{calc} is a vector of computed traveltimes, $\mathbf{s}$ is a vector of slowness parameters, and $\mathbf{D}_x$ and $\mathbf{D}_z$ are first-order finite-difference operators that define the variation in the solution in the horizontal plane and vertical direction, respectively. The penalty parameters, λ_1^2 and λ_2^2, control the weight of each functional on the solution with respect to fitting the data. The linearization of Eqn. 4 results in the regularized tomographic linear system shown in Equation 5.

$$\begin{aligned} \mathbf{A}\delta\mathbf{s} &= \delta\tau \,, \\ \lambda_1 \mathbf{D}_x \delta\mathbf{s} &= -\lambda_1 \mathbf{D}_x \mathbf{s} \,, \\ \lambda_2 \mathbf{D}_z \delta\mathbf{s} &= -\lambda_2 \mathbf{D}_z \mathbf{s} \,, \end{aligned} \tag{5}$$

In this linear system $\mathbf{s}$ is the current slowness model, $\delta\tau$ is the traveltime residual for the current model, and $\delta\mathbf{s}$ is the model perturbation to be determined. The entries of the tomographic matrix $\mathbf{A}$ are:

$$A_{ij} = \int_{i-th\,ray} W_{ij}(\mathbf{X}) d\mathbf{X} \tag{6}$$

where W_{ij} is the interpolation weight (Eqn. 1) along the i'th ray of the j'th slowness parameter, s_j.

The system of equations shown in Eqn. 5 is solved using conjugate gradients for least squares (Spakman and Nolet, 1988).

Continuation Method

Equations 4 and 5 show that the penalty terms, λ_1^2 and λ_2^2, control the weight of the regularization on the solution. The values of these parameters relative to the norm of the $\mathbf{A}$ matrix control the trade-off between fitting the data and satisfying the regularization constraints. The continuation method (Bube and Langan, 1994) is a strategy for relaxing these parameters in a systematic fashion during the inversion. Starting from high values (relative to the Frobenius norm of the $\mathbf{A}$ matrix) the penalty terms are relaxed each "continuation step" producing a family of solutions indexed by the values of λ_1^2 and λ_2^2. In a single continuation step, where the values of the penalty terms remain fixed, linear iterations are performed until the norm of the residuals does not decrease by a significant amount. Following this the values of the λ_1^2 and λ_2^2 are decreased and the next continuation step is performed. The inversion proceeds in this manner until the instabilities in Eqn. 5 produce a model so rough that the two point raytracing fails. A optimal solution can be singled out from the family of solutions by observing the trade-off between fitting the data and obeying the regularization constraints.

EXAMPLES

2.9-D traveltime tomography was performed on data collected in two experiments performed in the McElroy field in west Texas. In the first example we perform a joint inversion of direct-arrival traveltime data from three crosswell surveys collected in a triangular pattern. In the second example data collected in a more traditional manner, between two wells only, are inverted using the 2.9-D approach to obtain a thin 3-D slice. This slice is defined thick enough to include the 3-D geometry of the well deviations. The goal of this processing approach is to obtain accurate velocity tomograms for use in a time-lapse CO_2 injection monitoring experiment.

Figure 2 shows the well locations of the surveys used in our examples. The three surveys used for the first example are the post-injection surveys collected between JTM-661&1202, JTM-661&1080, and JTM-1080&1202. The pre- and post-injection surveys used in the second example were recorded between the wells JTM-1202 and JTM-1080. The initial model used in the inversion of both examples is homogeneous with a velocity of 15 kf/s. The ratio between the parameters $\lambda_2^2 / \lambda_1^2$ was fixed at 0.25 and the initial value for λ_1^2 was 3.0 in all inversions.

The traveltime data was obtained using a technique designed to improve the signal-to-noise ratio of the direct arriving energy. To accomplish this the seismic data were preprocessed by picking the direct arrivals, aligning the data using these picks, mixing along several traces and dealigning the data. New traveltime picks were then obtained from this enhanced data and the process was repeated in an iterative fashion, expanding the mixing operator each time, until the data quality was sufficient for reliable identification of the first breaks.

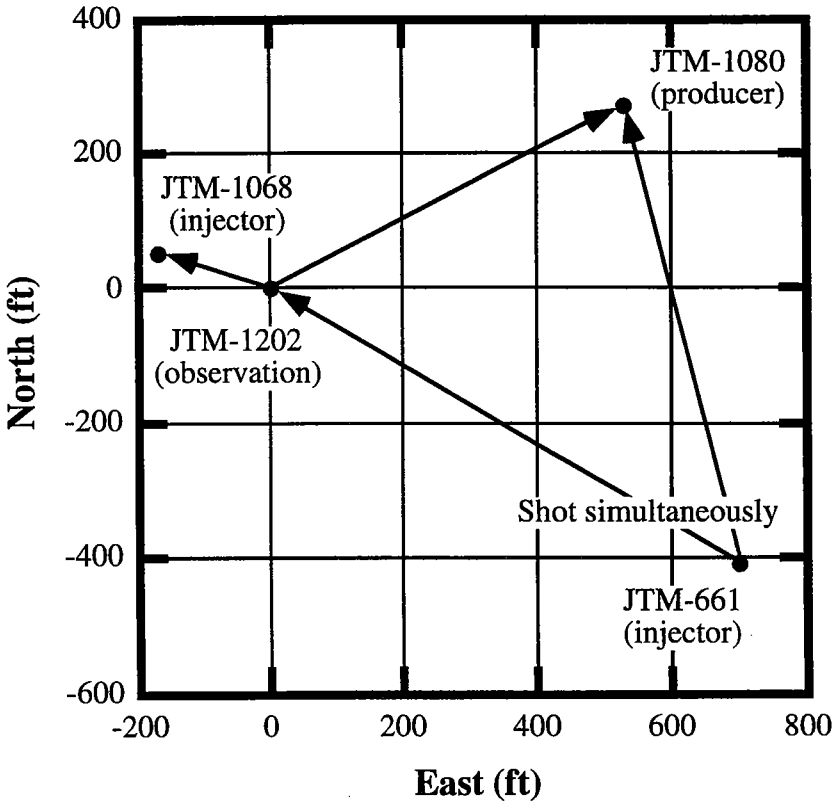

Figure 2: Well locations and shooting directions of the post-injection McElroy crosswell surveys. The three large offset surveys are used for 2.9-D tomography shown in the first example. The pre- and post-injection surveys collected between wells JTM-1080&1202 are used in the second inversion example.

Joint Inversion of the Post-Injection McElroy Surveys

The 2.9-D traveltime inversion algorithm was applied in a joint inversion of the three large offset surveys shown in Fig. 2. Traveltime data obtained from traces with source-receiver offsets less than 100 ft were not used in this inversion. This helps avoid low velocity zones where multiple arrivals can occur. Our 3-D two-point raytracing converges to a single event which depends on the initial model. Since the particular path calculated in zones where multiple arrivals are possible cannot be pre-determined there is the possibility of incorrectly matching traveltime picks with the wrong raypaths. The inclusion of this inconsistent data degrades the least-squares inversion.

A second difficulty is that these multiple surveys do not provide uniform ray throughout the reservoir region. Unfortunately, due to acquisition problems, the maximum depth of the source coverage was limited to just above the reservoir (~2900 ft) in JTM-661. In spite of the incomplete coverage, the regularization used in our algorithm prevents the inversion from becoming unstable. The main drawback of the coverage problem is that it reduces the lateral resolution inside the reservoir zone, especially near JTM-661.

Figures 4 and 5 show the 3-D velocity tomogram after 5 continuation steps. The rms of the residual traveltime of the joint inversion is 0.6 ms. The layer cake geology of the region is readily evident from the 2.9-D tomogram. There does appear, however, to be some lateral change in the reservoir zone. This suggests the possibility of CO_2 invasion within this region. Unfortunately pre-injection surveys were not collected in this triangular configuration which prevents a direct time-lapse comparison.

Time-lapse tomography in the McElroy field

In the second example we compute the time-lapse velocity difference for the repeated survey collected between wells JTM-1202 and JTM-1080. The model used in this inversion is a subset of the mesh model used in the first example that connects these two wells. These surveys have sources and receivers all across the reservoir zone. The pre-injection survey was modeled with an rms error of 0.3 ms and the post-injection tomography rms residual was 0.4 ms. These errors correspond to approximately 0.1% of the average traveltime values used for inversion. Figure 6 shows the percent velocity decrease relative to the pre-injection tomogram and Figure 7 shows the corresponding increase in velocity. Only differences above 3% were plotted. Figure 6 shows two anomalies. A streak anomaly representing a decrease in velocity at 2750 ft and a lateral gradient anomaly velocity decrease at the reservoir zone. The main feature in Fig. 7 is the streak anomaly of velocity increase just on the top of the reservoir. The two streak anomalies in Figs. 6 and 7 correlate with a thin low-velocity zone and a thin high-velocity zone on the well log respectively. Before jumping into geological interpretations for these two anomalies we need to investigate other less exciting interpretations such as picking problems with head waves. On the other hand, the large velocity decrease inside the reservoir is a less ambiguous consequence of the injection experiment.

DISCUSSION

The 3-D interpolation of tomograms is important for practical applications of crosswell tomography for high resolution reservoir characterization. The proposed method is a consistent approach for the estimation of a 3-D slowness model from crosswell surveys. The constraints on the scale of lateral variations certainly restrict the horizontal resolution of the solutions but at the crosswell scale these assumptions are not too far from geology in most cases of interest. The meaningful results of the McElroy surveys inversion indicate the potential advantages of moving crosswell interpretation to 3-D. This is a work in

progress. Additional tests with synthetic data using complex 3-D models should be performed to determine the limitations of this approach.

REFERENCES

Mathisen, M. E., Cunningham, P., Shaw, J., Vasiliou, J. H., Justice, J. H. and Guinzy, N. L., 1995, Crosswell seismic radial survey tomograms and the 3-D interpretation of a heavy oil steamflood: Geophysics, **60**, 651–659.

Bube, K. and Langan, B., 1994, A continuation approach to regularization for traveltime tomography: Expanded Abstracts, SEG Meeting, 64, 980–983.

Moser, T. J., Nolet, G. and Snieder, R., 1992, Ray bending revisited, BSSA, 82 (1), 259-288.

Harris, J. M., 1994, An approach to adaptive gridding for traveltime tomography. STP-**5** report, Paper D.

Press, W. H., Flannery, B. P., Teukolsky, S. A. and Vetterling, W. T., 1990, Numerical recipes, Cambridge University Press, NY.702p.

Spakman, W. and Nolet, G., 1988, Imaging algorithms, accuracy and resolution in delay time tomography. In: Mathematical Geophysics. Editors: Vlaar, N.J., Nolet, G., Wortel, M.J.R. and Cloetingh, S.A.P.L. Dordretcht. D. Reidel Publishing Company. 407P.

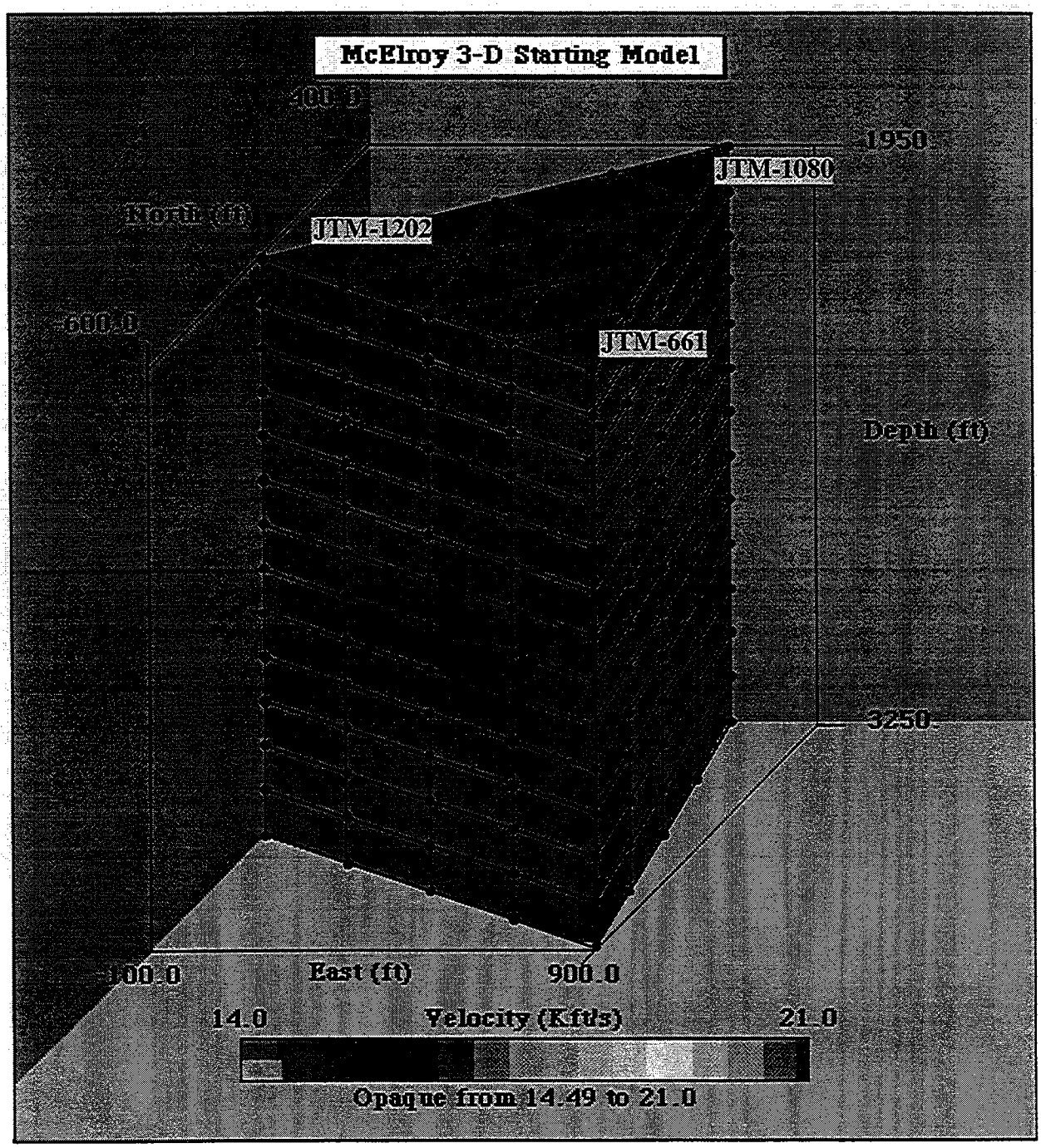

Figure 3: Initial model for the 2.9-D tomography. The depth interval between the nodes is 10 ft.

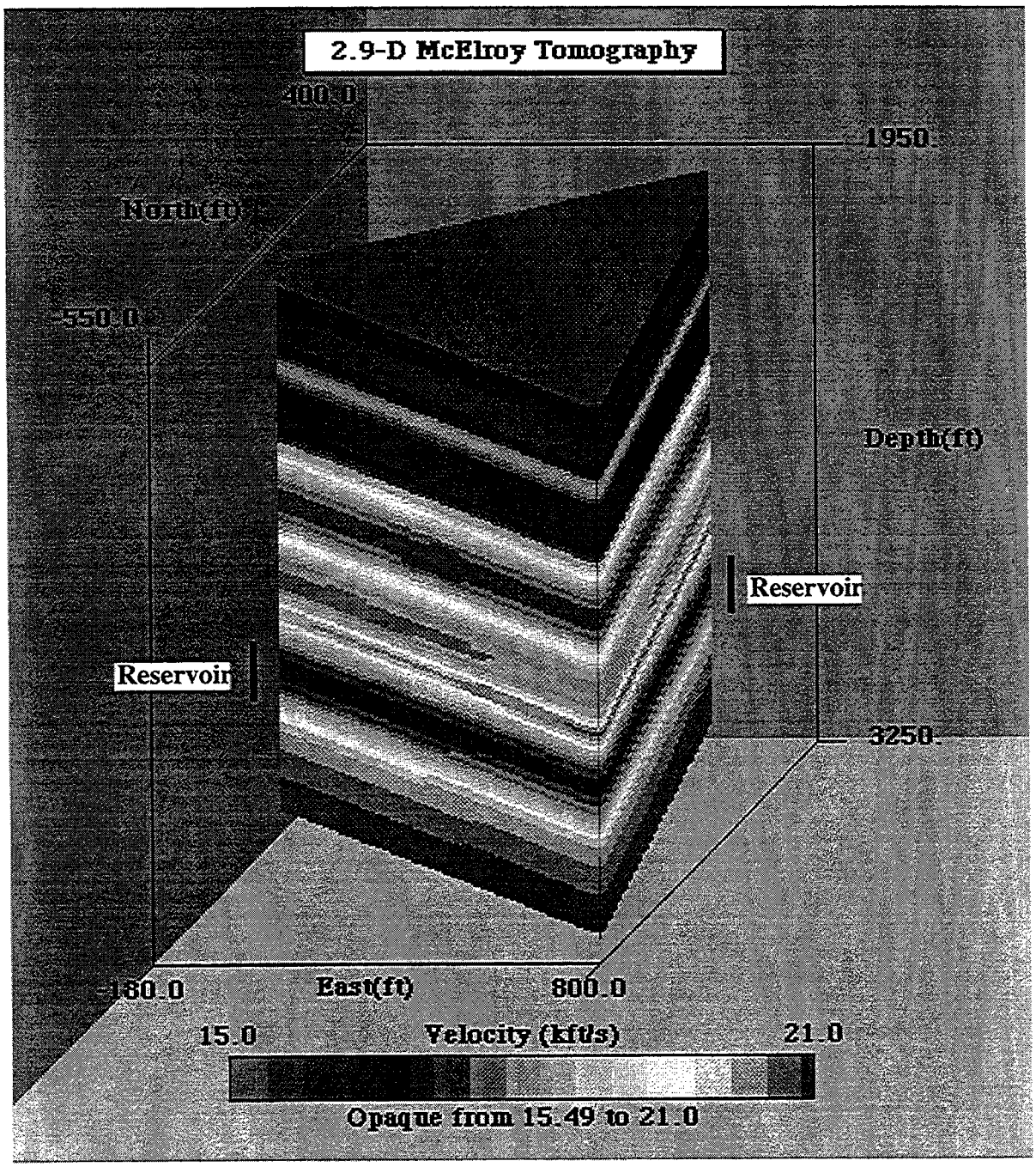

Figure 4: McElroy 3-D velocity tomogram after 5 continuation steps.

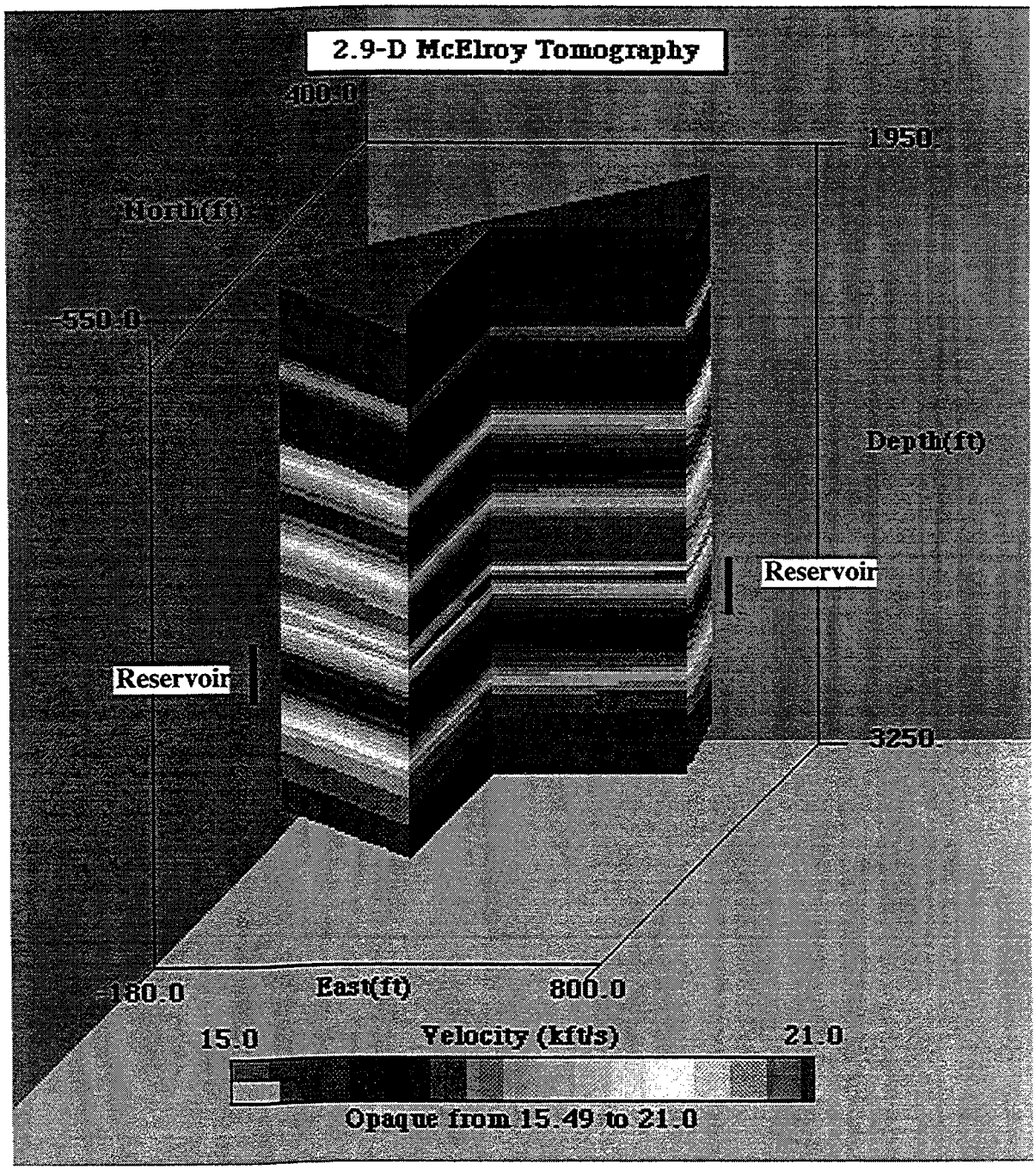

Figure 5: Cut Block view of the 3-D McElroy velocity tomogram. The lateral variations inside the reservoir region are better seen in this representation.

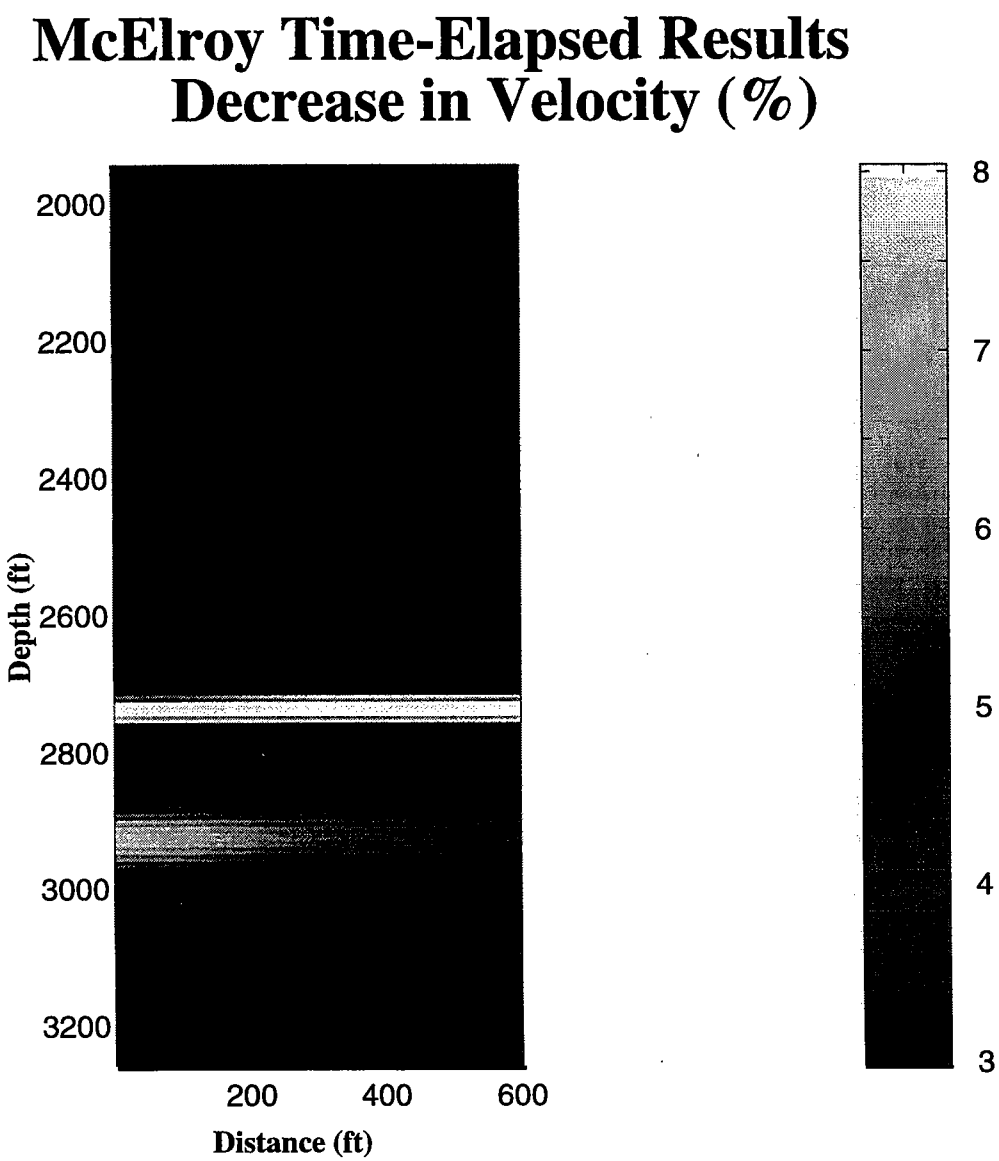

Figure 6: Percent decrease in velocity for the JTM-1080&1202 McElroy survey. Notice the decrease in velocity across the reservoir zone.

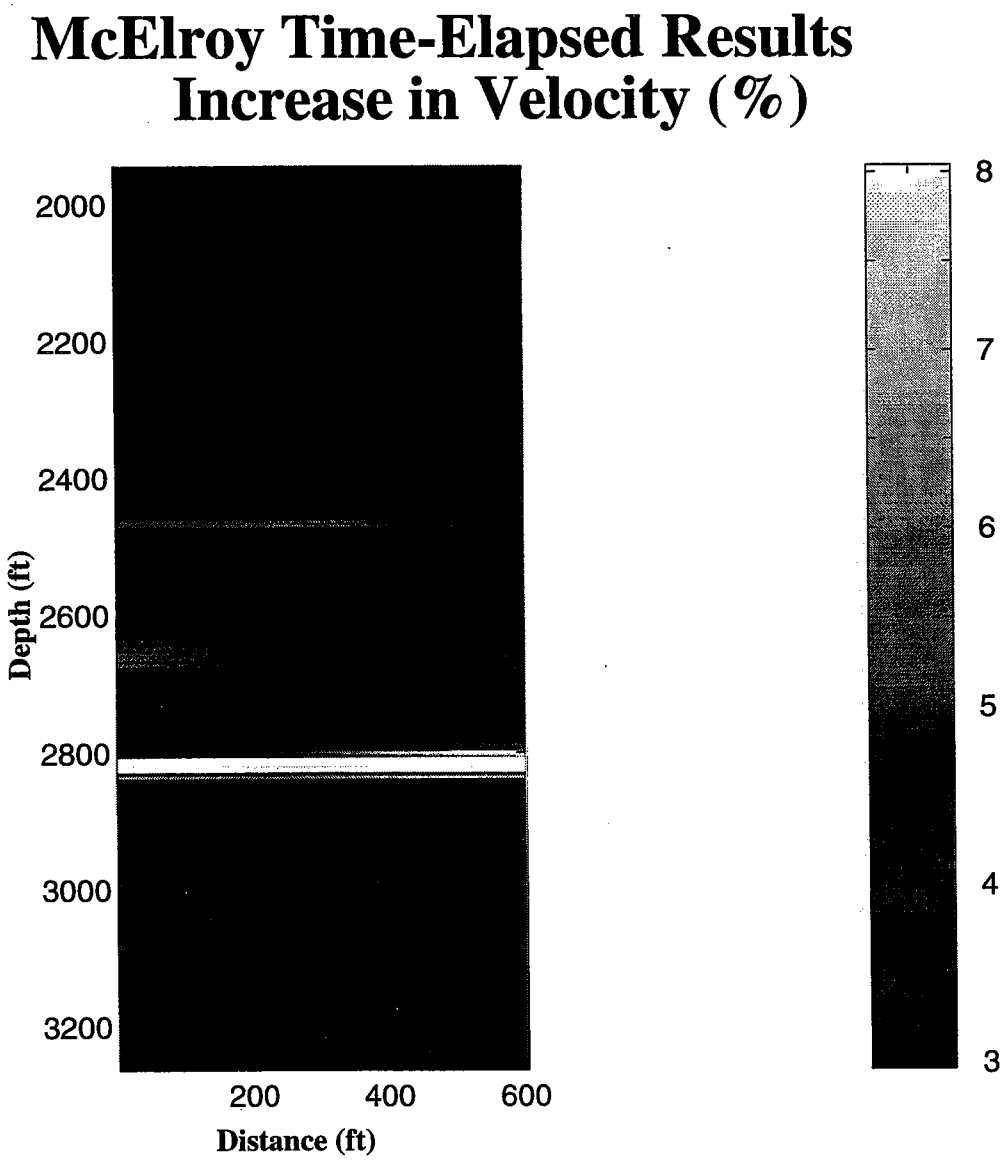

Figure 7: Velocity increase between the two far offset McElroy surveys. A high velocity streak at 2800 ft depth is the main feature.